An experimental study of sorption/desorption of selected radionuclides on carbon nanomaterials: a quest for possible applications in future nuclear medicine

Andrey G. Kazakov[a,b], Bogdan L. Garashchenko[a], Ruslan Yu. Yakovlev[a,*], Sergey E. Vinokurov[a], Stepan N. Kalmykov[a,b], Boris F. Myasoedov[a]

[a] *Vernadsky Institute of Geochemistry and Analytical Chemistry, Russian Academy of Sciences, Moscow, Kosygin st., 19, 119991, Russia*
[b] *Lomonosov Moscow State University, Chemistry Department, Moscow, Leninskie Gory, 1, 119991, Russia*

ABSTRACT

In this study, the possibility of application of carbon nanomaterials (CNMs) as carriers of various isotopes for nuclear medicine is investigated. The sorption of ^{99m}Tc, ^{207}Bi (as analog for ^{213}Bi), ^{90}Y, and ^{226}Ra (as analog for ^{223}Ra) in aqueous solutions with pH 6 and 0.01 M phosphate-buffered saline with pH 7 was studied on the following CNMs samples: detonation nanodiamonds (NDs), reduced graphite oxide (rGiO), and multi-walled nanotubes (MWCNTs). Commercial, hydrogenated, and aminated ND and hydrogenated MWCNTs adsorb Tc (VII) by 40–70%; however, in physiological saline, it is readily desorbed within 0.5 h. The sorption of Tc(IV) on commercial and carboxylated ND, as well as rGiO, was 60–90%. In this case, desorption in the biological media did not exceed 5% for each sample in 5 h. The sorption of Bi(III) on all the samples studied was from 80% to 100%, and the Bi(III)@ND conjugate was the most stable, as its desorption in the model biological medium was 4% for 5 h. It was shown that the sorption and desorption for Y(III) differs significantly depending on the CNM sample used, thereby allowing for the selection of the conditions for the use of Y(III)@CNMs conjugate for specific medical tasks. It was found that Ra(II) sorption occurs only on the rGiO sample and reaches 60%; however, depending on the medium, desorption was from 35% to 70% in 30 min, thereby complicating the use of the Ra(II)@rGiO conjugate. The data regarding sorption behavior and stability in biological media of the studied isotopes on CNMs allow us to not only choose the conditions for their effective use in nuclear medicine, but also evaluate the sorption behavior of other nuclear medicine isotopes.

1. Introduction

The rapid development of nuclear medicine in the field of molecular imaging of pathological organs and the targeted delivery of drugs poses the challenge of finding new effective nanomaterials. Carbon nanomaterials (CNMs) — nanodiamonds (NDs), graphene and its oxide (GO), carbon nanotubes (CNTs) — have unique structures and physicochemical properties for a wide range of applications in medicine [1].

Modern cancer treatment methods have a number of limitations associated with the presence of serious toxic and side effects of chemotherapy, radiation therapy, and targeted therapy with antibodies at the terminal stages of cancer development [2]. The use of CNMs offers new possibilities for the simultaneous detection and treatment of cancer. Most research regarding the therapeutic use of CNMs focuses on the targeted delivery of anticancer drugs and selective tumor

irradiation [3]. The size of CNMs varies from a few nm to hundreds of nm and is comparable to biological macromolecules such as proteins, enzymes, and DNA plasmids [4]. Therefore, CNMs can penetrate cell membranes, presumably during endocytosis [5], allowing them to act as drug carriers [6]. The nanosize of CNMs also allows them to penetrate and selectively accumulate in tumors at much higher concentrations than in surrounding healthy tissue [7,8]. They are retained owing to the abnormal structure of the capillary network in combination with a slow outflow through the undeveloped lymphatic system of the tumor (EPR effect).

Applications of NDs [9], graphene, multilayer graphene and its oxides [10], and CNTs [11] and their polymer derivatives as sorbents for the isolation of toxic elements from aqueous media are known. It has been shown that CNMs are characterized by fast sorption kinetics, high adsorption capacity, efficiency over a wide pH range, and consistency

with BET models and Langmuir and Freundlich isotherms [12]. The high potential of CNMs as sorbents also lies in the possibility of directional functionalization of their surface. For example, CNTs functionalized with the hydrophilic groups —OH and –COOH demonstrated a high sorption of polar organic substances with a low molecular weight [13].

The use of nanomaterials, including CNMs, as carriers for the targeted delivery of radioisotopes for diagnosis and treatment in nuclear medicine as part of radiopharmaceuticals (RP) is limited [14–25].

NDs with functionalized amino groups were used as carriers of [18]F [19]. These authors showed that such a drug can change its biodistribution when surfactants are added and the surface charge of nanoparticles changes.

Graphene modified with polyethylene glycol was used as a carrier for the ^{131}I radionuclide, thereby providing an increased efficiency against cancer cells than the free ^{131}I isotopes [20]. Sorption of [225]Ac on dextran-modified graphene for delivery to tumor angiogenic vessels was studied [21]. [99m]Tc was immobilized on GO, modified with DOTA (1,4,7,10-tetraazacyclododecane-1,4,7,10-tetraacetic acid), and the degree of labeling was > 90% [22].

It was shown that single-walled CNTs (SWNTs), modified with a tumor-specific chelating agent with ^{111}In and a fluorescent label, can successfully deliver a radionuclide into cells [23]. In [24] [211]At was effectively sorbed inside the SWNTs due to the van der Waals interactions. It was shown that [225]Ac and [89]Zr in the composition of RP based on functionalized SWNTs reduced the tumor volume of a human colon adenocarcinoma [25]. In another study, multi-walled NT (MWCNTs) cavities were filled with Na[125]I, and were successfully imaged in mice using computed tomography [16]. Using the ^{99m}Tc label, the biodistribution of oxidized MWCNTs and NDs separately and with the joint presence in the body was studied [17].

The sorption of elements on CNMs is ensured by physical adsorption, electrostatic interaction, surface interaction between surface functional groups, and the elements. For example, sorption onto a NDs is provided by a wide range of functional groups of various chemical natures. On sp^2-carbon graphene/graphite oxide and MWCNTs it is possible because of the direct covalent intrasphere bonds that are formed between deprotonated functional groups on the surface, or electrostatic bonds of the outer sphere formed between the surface and a radionuclide surrounded by a hydration sphere of water molecules [26]. Owing to chemical modification of the surface of CNMs, other sorption interactions are possible [27]. Thus, oxidation and reduction play significant roles in the interactions between the CNM surface and radioactive element.

This study addresses the sorption/desorption of the nuclear medical isotopes of technetium, bismuth, yttrium, and radium on different CNMs for potential use as carriers for their targeted delivery. To this end, the adsorption behavior of Tc(VII,IV), Bi(III), Y(III), and Ra(II) were studied on commercial ND, reduced graphite oxide (rGiO), and MWCNTs samples and its oxidized and reduced derivatives. The choice of isotopes is determined not only by the wide spectrum of their application, but also by the difference in their chemical properties. Interest in CNMs of different structures is because of some of their advantages: different biodistribution, different rate of accumulation in the tumor, the degree of retention of the radionuclide, the potential biocompatibility of their individual forms, the possibility of their synthesis in industrial volumes, and their low cost compared to vector molecules.

2. Experimental design

2.1. CNMs and their characterization

Commercial samples of the following CNMs were used: ND powder (SKTB «Technolog», Russia, trade mark UDA-TAN), rGiO aqueous suspension, and MWCNTs powder («NanoTekhTsentr» Ltd., Tambov,
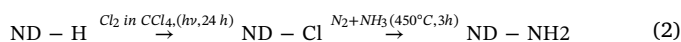
Russia). IR spectroscopy, X-ray photoelectron spectrometry (XPS), and X-ray diffraction (XRD) data for commercial samples of CNMs are provided in the Supplementary material. Particle morphology of CNMs was determined by high resolution TEM (HRTEM) using a JEOL JEM-2100F/Cs/GIF (200 kV, 0.8 A). To determine impurity elements in CNMs, ICP-MS (X Series 2, Thermo Scientific, USA) analysis and gamma activation analysis were used [28].

The elemental surface composition of CNMs was determined by XPS using a Kratos Axis Ultra DLD (Kratos Analytical Ltd., United Kingdom). AlK$_{\alpha1.2}$ (hν = 1486.6 eV) radiation under vacuum of $5 \cdot 10^{-7}$ Pa at room temperature was used. The calibration of photoelectron peaks was conducted along the C1s carbon line with a binding energy of 285 eV and normalized to the content of all detected elements.

The hydrodynamic particle diameter of CNMs in hydrosols was determined by dynamic light scattering (DLS) on a ZetaSizer Nano ZS analyzer (633 nm) ZEN 3600 (Malvern instruments, Ltd., USA).

Potentiometric titration was used to determine the acidic-functional groups on the surface of CNMs. A reaction with 2,4,6-trinitrobenzenesulfonic acid (TNBS) with preliminary calibration by glycine was carried out with spectrophotometric detection (λ = 408 nm) to estimate the number of amino groups.

Modification of ND samples - oxidation, hydrogenation, chlorination and amination - was carried out by reactions 1–3 according to the methods [29,30]. Hydrogenation of rGiO (hydrogenated rGiO – h-rGiO) and MWCNTs (rMWCNTs) took place under similar conditions, while the aqueous suspension of rGiO was previously dried. All chemical reagents used in the work had a purity that was not lower than "chemically pure."

$$ND \xrightarrow{10\%H_2 + 90\%Ar \ (800°C, 5h)} ND - H \tag{1}$$

$$ND - H \xrightarrow{Cl_2 \ in \ CCl_4, (h\nu, 24 \ h)} ND - Cl \xrightarrow{N_2 + NH_3 (450°C, 3h)} ND - NH2 \tag{2}$$

$$ND \xrightarrow{H_2SO_4 / HNO_3 \ (3:1), (120°C, 24 \ h)} ND - COOH \tag{3}$$

2.2. Radiotracers and detection

The isotopes [99m]Tc ($T_{1/2}$ = 6 h), [207]Bi ($T_{1/2}$ = 31,6 y), [90]Y ($T_{1/2}$ = 64 h) and [226]Ra ($T_{1/2}$ = 1600 y) were used in the experiments. [99m]Tc was obtained from a [99]Mo/^{99m}Tc generator, manufactured in the Karpov Institute of Physical Chemistry, Obninsk, Russia. [99m]Tc(VII) was eluted from the generator with physiological saline, after which it was diluted with bidistilled water at least 1000 times. [207]Bi was obtained from Cyclotron Co., Ltd., Obninsk, Russia in a solution of 0.1 M HCl without a carrier. An aliquot of the [207]Bi solution was evaporated to dryness and dissolved in an ammonia buffer at pH 6. [90]Y was separated from the solution of ^{90}Sr by sequential separation by extraction chromatography using SR resin and RE resin (Triskem, France) according to the method [31]. [90]Y was separated in 0.05 M HNO$_3$ medium, the solution was evaporated and dissolved in 0.01 M phosphate-buffered saline (PBS) at pH 7. A solution of radium-226 was obtained by dissolving [226]RaBr$_2$ (0.1 mg) in 0.01 M HCl, and aliquots of the resulting solution were diluted with double distilled water 100–1000 times. Solutions of radionuclide during sorption had the following concentrations: [99m]Tc – 10^{-13} M, [207]Bi – 10^{-9} M, [90]Y – $4 \cdot 10^{-14}$ M, and [226]Ra – 10^{-6} M.

Isotopes ^{99m}Tc, [207]Bi and [226]Ra were registered by their gamma radiation on a gamma-ray spectrometer with high-purity germanium detector GR 3818 (Canberra Ind, USA). [90]Y was detected on a GreenStar beta spectrometer (Russia) using an UltimaGold liquid scintillator (PerkinElmer Inc.).

2.3. Sorption experiments

The sorption of the studied radionuclides in an aqueous solution with pH 6 or in PBS was studied on suspensions containing 1 mg/mL of

CNMs. A solution of the selected medium was placed to the Eppendorf tubes, then an aliquot of the CNMs suspension and the radiotracer were added, so that the volume of the resulting solution in each case was 1 mL. The experiments were carried out at a temperature of 25 or 37 °C, which was controlled by a shaker thermal attachment (TS-100, Biosan, Latvia). After sorption, the phases were separated by centrifugation for 20 min at 18,000*g* (CM-50, Eppendorf, USA), 100 μl of the supernatant were taken, and the gamma- or beta-spectrum were registered.

To study the sorption of Tc(IV), the pertechnetate anion was preliminarily reduced with Sn(II) chloride according [32]. A weighted amount of $SnCl_2$ was dissolved in 0.02 M HCl, from which oxygen was previously removed by purging argon through it. An aliquot of the resulting solution was added to Eppendorf tubes before adding $^{99m}TcO_4^-$. The transition of tin-reduced Tc(IV) to the surface of CNMs was confirmed by parallel experiments under the same conditions without CNMs, making sure that upon centrifugation Tc(IV) only precipitated in the presence of CNMs.

Desorption of the studied radionuclides from CNMs was carried out in physiological saline, PBS or PBS containing 40 g/L of bovine serum albumin (BSA). Physiological saline is isotonic to blood plasma and is its simplest model. PBS also reflects the salt composition and has the same pH, and PBS + BSA imitates both salts and protein backgrounds of the blood plasma. Such media are usually used as biological models for desorption [33–35], and the dependence of the desorption on the composition of the selected medium allows for suggesting a possible mechanism of sorption.

3. Results and discussion

3.1. Characterization of CNMs

3.1.1. Characterization of commercial (initial) CNMs

It was found that the CNM samples studied differ significantly in size, structure, specific surface area, and impurity content (Table 1). Thus, ND is formed by spherical particles that have a crystalline structure. The size of primary ND particles varies between 3 and 10 nm, with an average of 4–6 nm (Fig. 1A, B). ND particles are surrounded by a non-crystalline shell, which represents a broken diamond crystal lattice in sp^3 hybridization. A commercial rGiO sample is a mixture of flat micron-sized flat sheets (Fig. 1C) with a thickness of approximately 1–10 graphene layers and dispersed rGiO in the form of particles with sizes of approximately 2 nm (Fig. 1D). MWCNTs are randomly curved filiform multilayer graphene layers of a cylindrical shape with an internal closed cavity, a diameter of up to 30 nm, and a wall thickness of

Table 1
Characterization of CNMs.

Characteristics	ND	rGiO	MWCNTs
Particle size of the original samples (nm)	3–10	Nanosheets – 2 Sheets $> 10^2$	Length $> 2 \cdot 10^4$ Diameter – 30 Wall thickness 5–10
Total content of impurities according to ICP-MS (mg/g)	1.4	3.0	14.0
Main impurities (> 0.1 mg/g) and their content (mg/g)	Fe – 0.538 Ti – 0.459 K – 0.156	Ti – 2.600 Al – 0.124	Mo – 6.880 Co – 5.830 Al – 0.635 Ni – 0.156
Specific surface area (m^2/g)	240	700–1000	160
Elemental composition of the surface according to XPS	C (sp^3) – 92.3% O – 7.7% N – 1.0%	C (sp^2) – 77.4% C (sp^3) – 7.9% O – 14.7%	C (sp^2) – 99.0% O – 1.0%
Size of particles and their aggregates in hydrosols (nm)	100	Particles – 2 Sheets – n/d	n/d

5–10 nm (Fig. 1E, F). At the ends of the MWCNTs, catalyst particles are visible (Fig. 1E), as evidenced by the significant content (14 mg/g) of Co, Mo, and Ni, according to ICP-MS (Table 1). The content of the summarized impurities in ND and rGiO is significantly less (1.4 and 0.3 mg/g, respectively). Most of the impurities in ND are iron and titanium, and in rGiO is mainly titanium.

The free surface area according to the BET method, m^2/g for ND is 240, for rGiO is 700–1000, and for MWCNTs is 160 (Table 1).

The content of oxygen and nitrogen on the surface of ND, according to XPS, is 7.7 at.% and 1 at.%, respectively, and the remainder is carbon in sp^3 hybridization. The high oxygen content on the ND surface is determined by treatment with nitric acid when it is extracted from a diamond blend [36]. The oxygen content on the rGiO surface, determined by XPS, is 14.7 at.%, and the remaining is 77.4 at.% carbon in sp^2 hybridization and 7.9 at.% carbon in sp^3 hybridization. The presence of the sp^3 phase of carbon is apparently due to the destruction of oxidized graphene sheets. The content of elements on the MWCNTs surface is 99.0 at.% carbon in sp^2 hybridization and 1.0 at.% oxygen.

The state of CNMs in an aqueous solution also differs. NDs form aggregates with a size of 100 nm. rGiO nanosheets in the solution retain their size of 2 nm. The program of the equipment used does not calculate the size of the rGiO sheets, because their shape is far from spherical, which is consistent with [22]. It was noted that the particle size of MWCNTs in an aqueous solution also cannot be determined because it is impossible to obtain a stable suspension owing to their hydrophobicity.
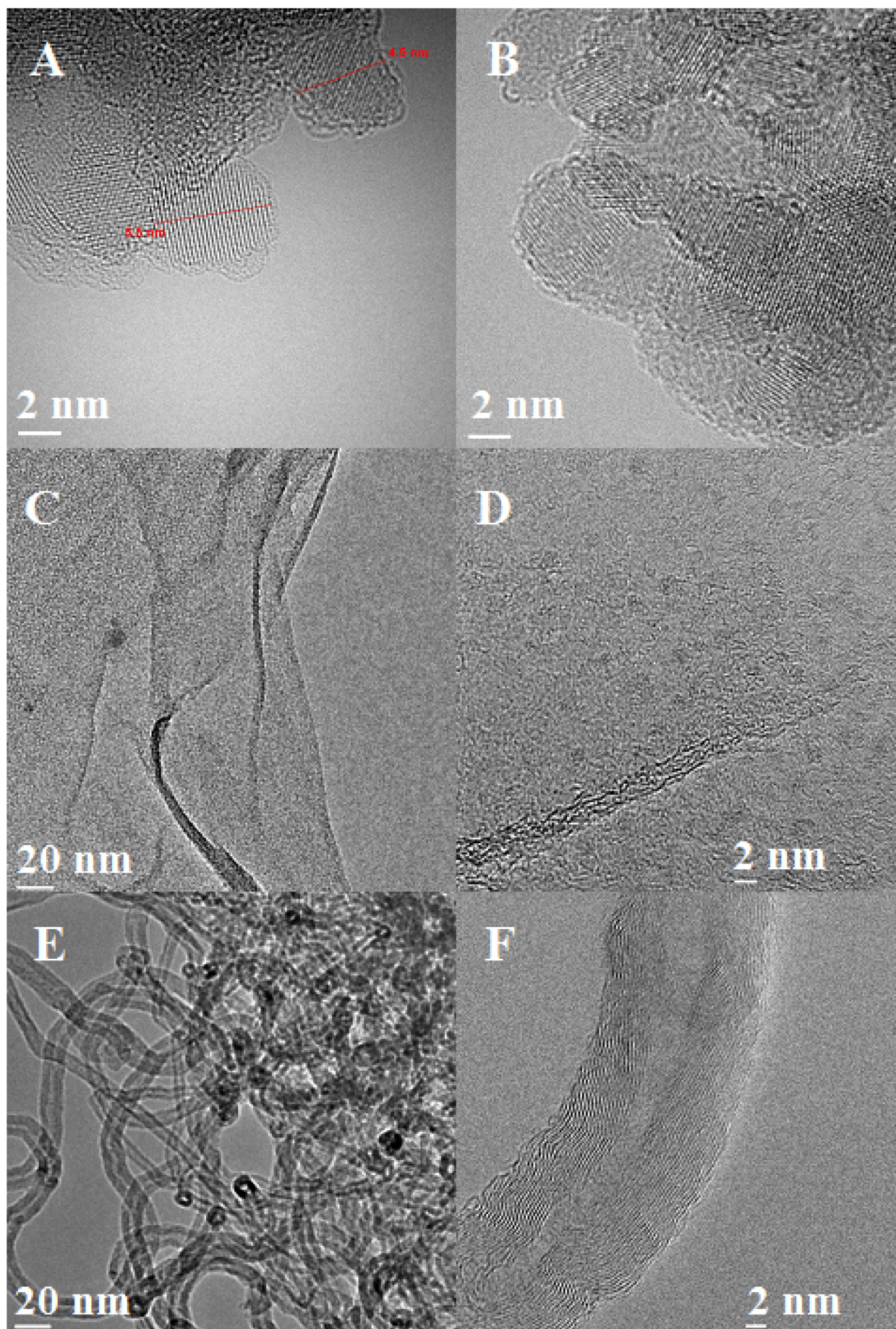
3.1.2. Characterization of modified CNMs

The modification of ND with hydrogen for 5 h at 800°C (reaction 1) leads to a decrease in the content of acidic groups from 330 to 20 μM/g. After annealing in a reducing atmosphere (reaction 1), the oxygen content on the h-rGiO surface decreased almost five times to 3 at.%, and for rMWCNTs, from 1.0 to 0.6 at.%. Moreover, the binding energy line, corresponding to molybdenum, does not appear on the spectra of rMWCNTs, which indicates the removal of Mo and other impurities of the catalyst as a result of hydrogenation to levels below the detection limit of the method. When the initial ND was treated with ammonia at 450°C (reaction 2) the number of amino groups formed was 120 μM/g. The effect of a mixture of nitric and sulfuric acids during the oxidation of ND (reaction 3) leads to an increase in the content of acid groups to 990 μM/g. The oxygen content in the ND-COOH sample is 9 at.%, which is only 1.3 at.% higher than in the commercial ND sample (Table 1). This indicates the likely similarity of the sorption behavior of the initial and oxidized ND samples.

It was found that the behavior of modified CNMs in aqueous solutions is different. Thus, the average size of ND-H, ND-NH$_2$, and ND-COOH aggregates was 50, 80, and 95 nm, respectively, and their zeta-potential was +30, +50, and +30 mV, respectively. Therefore, a change in the functional cover of the ND surface leads to a decrease in size and an increase in colloidal stability of the modified ND samples. At the same time, it was shown that h-rGiO particles form aggregates of two types, which correspond to a bimodal distribution with modes of 200 and 700 nm, and the zeta potential decreased from −46 to −10 mV. It is evident that a significant difference in the size distribution of rGiO and h-rGiO is due to the preliminary drying of rGiO before hydrogenation (reaction 1). It was found that upon hydrogenation, MWCNTs become more hydrophilic because they form a more stable suspension than a commercial sample. Like rGiO, rMWCNTs particles form aggregates of two sizes, which are approximately 150 and 650 nm and have a zeta potential of −7 mV.

3.2. Technetium sorption

^{99m}Tc is the most widely used diagnostic nuclide in nuclear medicine today. This is due to both the optimal nuclear physical properties for SPECT [37] (90% γ, $T_{1/2}$ 6 h), and the ability to obtain it from a

(caption on next page)

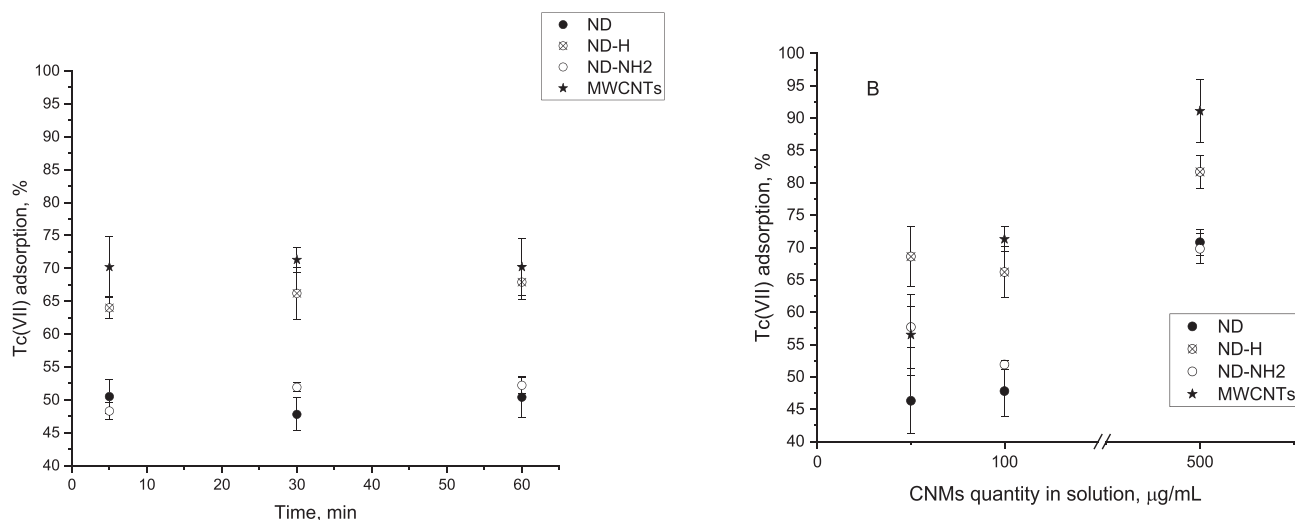**Fig. 1.** HRTEM micrographs of commercial samples of CNMs: ND (A, B), rGiO (C, D), and и MWCNTs (E, F).

Fig. 2. Sorption of Tc(VII) from an aqueous medium with pH 6 at 25 °C at 100 μg/mL (A) and at different sorbent contents (B).

$^{99}Mo/^{99m}Tc$ generator. Molybdenum-99 has a high probability of being formed during the fission of uranium during the operation of nuclear reactors, and its $T_{1/2}$ 60 h allows generators to be delivered to scientific and medical institutions over considerable distances. The RP based on ^{99m}Tc includes its anionic and cationic forms of various valence states [38].

3.2.1. Technetium(VII)

Sorption of $^{99m}TcO_4^-$ was previously studied on activated [39,40] and mesoporous carbon [41] and inorganic sorbents and minerals [42] for the purpose of environmental radioactive monitoring. It has been shown that activated carbon sorbs Tc(VII) better than the other carbon materials studied.

In this work, we studied the sorption of $^{99m}TcO_4^-$ milked from a $^{99}Mo/^{99m}Tc$ generator on CNMs samples. Sorption was carried out from an aqueous solution with pH 6. It was found that sorption of $^{99m}TcO_4^-$ on the ND, ND-H, ND-NH$_2$, and MWCNTs samples reached 50–70% (Fig. 2A). It was shown that equilibrium for all samples is reached within 5 min. A lack of sorption was observed on the rGiO, h-rGiO, and rMWCNTs samples. An increase in the sorption ability of the ND-H sample may be due to the formation of a high positive ζ-potential (+40 mV) on the surface and the electrostatic attraction of $^{99m}TcO_4^-$. The primary amino group is able to protonate and provide a positive surface charge, depending on which sorption of the $^{99m}TcO_4^-$ occurs at pH 1–9 [43]. In the case of ND-NH$_2$, however, there was no advantage in sorption capacity over commercial ND.

For the ND, ND-H, ND-NH$_2$, and MWCNTs samples, which sorbed Tc(VII), the dependence of the sorption value on the amount of sorbent in the sample was also studied (Fig. 2B). Fig. 2B shows that for all three samples of NDs, the sorption at an m/V of 50 and 100 μg/mL is constant and is c.a. 47% for ND, 58% for ND-NH$_2$, and 67% for ND-H. With a further increase in the m/V to 500 μg/mL, an increase of sorption of up to 70% for ND and ND-NH$_2$ and up to 82% for ND-H is observed. For MWCNTs, there is an increase in the sorption from 56 to 71%, with an increase in m/V from 50 to 100 μg/mL, and an increase of up to 91% with m/V 500 μg/mL.

It was previously shown that sorption of $^{99m}TcO_4^-$ on the surface of activated carbon may include two potential binding sites –OH and –C═O, which are part of the carboxyl group [44]. Moreover, for reduced forms of activated carbon, sorption can occur due to the electrostatic attraction of a positively charged solid surface and $^{99m}TcO_4^-$. Therefore, an increase in sorption on ND-H may be due to an increase in the

zeta potential from +30 mV to +50 mV, which contributes to a stronger retention of $^{99m}TcO_4^-$.

It was found that physiological saline quantitatively desorbs Tc(VII) from ND, ND-H, ND-NH$_2$, and MWCNTs samples at 25 °C after 30 min. These results indicate weak electrostatic interactions between the CNMs surface and the $^{99m}TcO_4^-$. It is likely that the quantitative desorption of Tc(VII) may be due to a decrease in the positive ζ-potential of the surface in the medium of physiological saline [44]. The introduction of additional complexing substances that bind $^{99m}TcO_4^-$ with CNMs or surface modification of CNMs is required to create a stable positive charge in salt media.

3.2.2. Technetium(IV)

Currently, technetium in nuclear medicine is used in RP mainly in cationic forms, Tc(IV,V) [38,45]. In this work, the oxidation state of technetium was not determined, but for nanoparticles, including CNMs, it is usually indicated on their surface as Tc(V) [17] or not indicated at all [22]. Tc(IV) is also formed upon reduction of Tc(VII) with tin chloride without the presence of a complexing ligand or carrier [45].

In the present work, Tc(IV) was obtained by adding a tin(II) chloride as a reducing agent to the $^{99m}Tc(VII)$ eluate. It was shown that the optimal tin concentration for the reduction of Tc(VII) was 10^{-6} M. Under these conditions, no visible tin precipitate is formed, and the activity during centrifugation for 20 min at 18,000 g does not change, which indicates that the presence of tin will not prevent the immobilization of ^{99m}Tc on the CNMs. Sorption of Tc(IV) on CNMs was studied in a PBS solution at 25 °C. It was established that ND and ND-COOH samples sorb approximately 90% of ^{99m}Tc, and the sorption process is characterized by fast kinetics, with equilibrium occurring in 5 min (Fig. 3A). This is due to the rapid reduction of pertechnetate with Sn(II) chloride to Tc(IV), which, presumably, is complexed with oxygen-containing CNMs groups. rGiO adsorbs Tc(IV) by 60–75%, but with an increase in sorption time to 60 min, a continued increase in the degree of sorption is observed, which indicates a slow kinetic process. Sorption in 60 min does not exceed 10% for h-rGiO, MWCNTs and rMWCNTs samples. This indicates the necessity for oxygen-containing groups on the surface of CNMs to immobilize Tc(IV). It was shown that with an increase in the m/V from 10 to 100 μg/mL for ND, ND-COOH and rGiO, the differences in the sorption do not exceed 10% (Fig. 3B). Therefore, while using CNMs as carriers of ^{99m}Tc in RP, it is possible to use microgram quantities of these materials, which solves the problem of minimizing potential negative effects on the body.
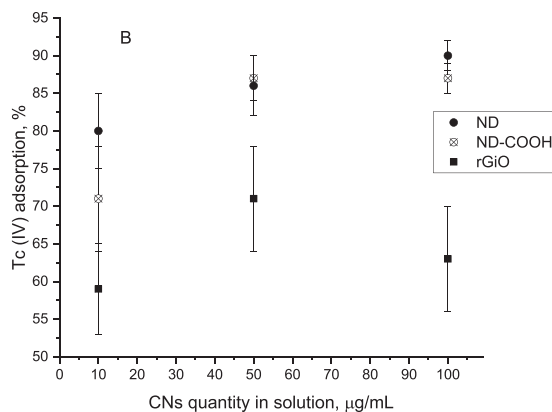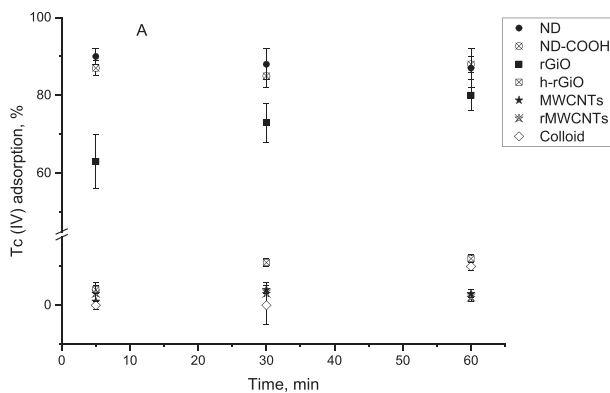
Fig. 3. Sorption of Tc(IV) from PBS at 25 °C at 100 μg/mL (A) and at different sorbent contents (B).

It was found that the desorption of Tc(IV) from the ND, ND-COOH, and rGiO samples in a PBS + BSA solution with a pH of 7 at 37 °C for 24 h does not exceed 5%. Thus, when introduced into the body, RP ^{99m}Tc(IV)@CNMs could be stable and be used for the targeted delivery of ^{99m}Tc.

3.3. Bismuth(III)

Bismuth isotopes ^{212}Bi and ^{213}Bi are used in nuclear medicine in targeted alpha therapy of cancer tumors [38]. The most optimal ways of their production are ^{225}Ac/^{213}Bi and ^{212}Pb/^{212}Bi generators [46–48]. Currently, tumor-specific peptides are used for immunotherapy with Bi (III) in RP [49,50]. For the first time, this work studied the possibility of using CNMs as carriers of bismuth isotopes.

It was found that the sorption of ^{207}Bi(III) by all CNMs studied is from 80 to 100% (Fig. 4). A kinetics study showed that sorption equilibrium for ND, ND-COOH, h-rGiO, and MWCNTs samples is achieved in 5 min, and for rGiO and rMWCNTs samples, in 30 min. Thus, it was noted that for the sorption of Bi(III) from aqueous solutions, in contrast to Tc(IV), the presence of oxygen-containing groups on the CNMs surface does not have a decisive influence on the efficiency of sorption.

It is particularly noted that with a decrease in the m/V to 10 μg/mL, the degree of sorption decreases slightly (up to 5%). This allows the use of small amounts of CNMs in RP for sorption of Bi(III), which reduces the potential toxic burden on the body.

It was found that ND, ND-COOH and rGiO show the highest resistance to Bi(III) desorption (Fig. 5). Among them, ND was chosen for experiments on desorption under conditions close to biological. It was found that in PBS + BSA solution at 37 °C after 5 h, no > 4% Bi(III) is desorbed from ND, and up to 20% in 18 h. The experimental data
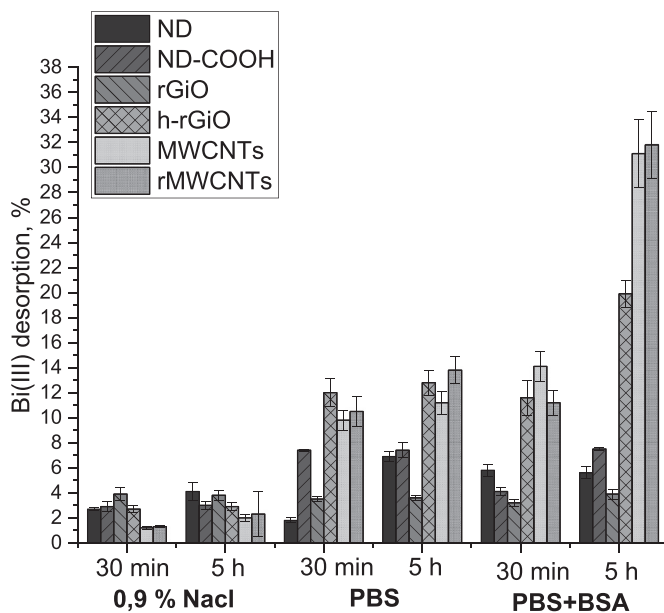

Fig. 5. Desorption of Bi(III) in various media at 25 °C, 100 μg/mL CNM content.

obtained create the prerequisites for the effective use of CNMs in the composition of RP with Bi(III).

3.4. Yttrium(III)

Yttrium has two isotopes that have found application in nuclear medicine, and these are ^{90}Y (T$_{1/2}$ 64 h), and ^{86}Y (T$_{1/2}$ 14,7 h) [38]. The first is a pure beta-emitter, and has found widespread use in therapy, where it is usually bounded with peptides or antibodies [51]. The advantage of the isotope is its availability because it is easily obtained from the ^{90}Sr/^{90}Y generator. ^{86}Y emits positrons, and can be used in PET for the imaging of ^{90}Y in the body [52].

According to the results of the studies, the highest sorption of ^{90}Y with fast kinetics, 99 and 98%, was shown by commercial ND and ND-COOH, respectively (Fig. 6). Moreover, after 15 min, 84% of Y(III) was adsorbed on ND and 90% of Y(III) on ND-COOH, and then sorption equilibrium was gradually established over 24 h. The rGiO sample showed slower kinetics, whereby 66% was adsorbed within 15 min, 70% within 1 h, and sorption increased to 93% within 24 h. Simultaneously, a significant decrease in sorption capacity was observed for the h-rGiO sample, which is associated with the absence of oxygen-containing groups compared to rGiO and therefore, in 60 min h-rGiO no > 48% Y(III) is sorbed, while the sorption value does not change
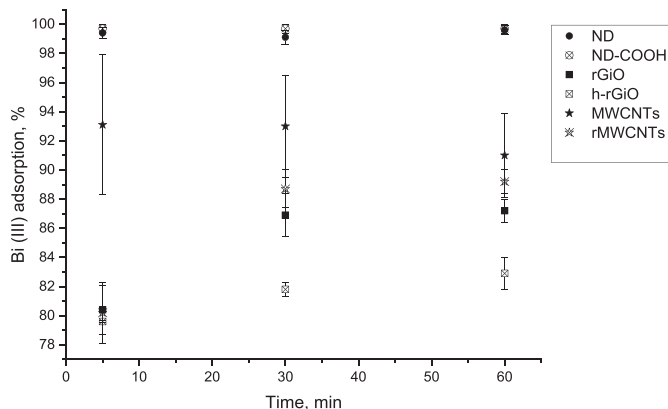

Fig. 4. Sorption of Bi(III) in an aqueous medium with pH 6 at 25°C, 100 μg/mL CNM content.
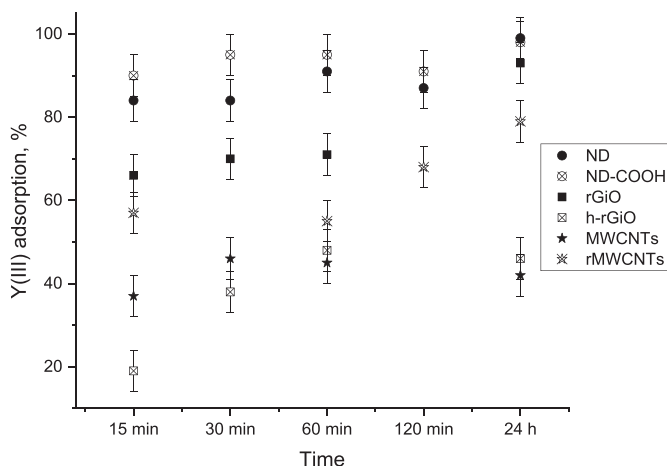
Fig. 6. Sorption of Y(III) in PBS at 25 °C, 100 μg/mL CNM content.

after 24 h (Fig. 6). MWCNTs also showed a weak ability to sorb Y(III) and adsorbed 46% after 30 min, after which equilibrium was observed at 24 h (Fig. 6). It should be noted that the modification of MWCNTs during hydrogenation (reaction 1) leads to an increase in the degree of Y(III) sorption and therefore, in 24 h, sorption reached 79% (Fig. 6). This may be due to the opening of MWCNTs channels during such processing due to the presence of a small oxygen impurity in the gas mixture, which acidifies and opens their ends. It was previously shown that in the process of hydrogenation there is a decrease in the number of structural defects, and the removal of catalyst metal impurities [53].

It can therefore be assumed that Y(III) adsorption on rGiO and MWCNTs can proceed by at least two mechanisms: (1) fast adsorption on the external surfaces of MWCNTs, and (2) slow adsorption in the internal channels of MWCNTs, the distribution of which depends on the time the sample was in solution. This is in concordance with other work [54], in which 90% of Eu(III) was adsorbed on MWCNTs, and then sorption slowly increased over time.

It was shown that the highest desorption in PBS + BSA solution reaches 35% within 15 min (except rMWCNTs – 60%), and then desorption did not change within 1 h (Fig. 7). In the first min of contact of the nanoparticles with the protein, weakly bound Y(III) is therefore removed from the surface of rGiO. In 15 min, 27% Y(III) is desorbed with ND, ND-COOH. For rGiO and h-rGiO, 15 and 20% of ^{90}Y was
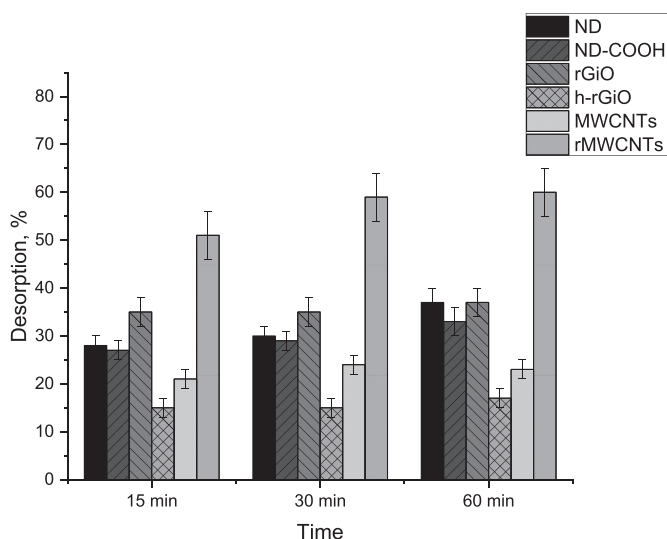
desorbed after 15 min. If we take into account that CNMs rapidly accumulate in organs [55–57], this time is sufficient to deliver Y(III) to the desired location.

According to the data obtained, two sorption mechanisms could be assumed: (1) chemisorption with the formation of ^{90}Y complexes with oxygen-containing groups (-COOH, -OH) on the rGiO surface, and (2) physical adsorption due to electrostatic attraction between Y(III) and oppositely-charged groups on the surface.

Desorption of Y(III) from MWCNTs was 21% in 15 min and did not change for 1 h. For rMWCNTs, desorption was the highest at 51% in 15 min, and 60% in 60 min. This may be due to the fact that the density of defects in the surface of MWCNTs decreased as a result of annealing [58]. Therefore, the number of strong adsorption sites in rMWCNTs is decreased.

3.5. Radium(II)

The alpha-emitting isotope ^{223}Ra with $T_{1/2}$ 11.4 d is used in the treatment of bone metastases in prostate cancer and in breast cancer [38]. Radium is a calcium mimic, and therefore, when ingested, it mainly accumulates in the bones [59]. The difficulties with the chelation of divalent radium create barriers for the creation of RP with targeted delivery, so only radium-223 chloride solution is currently used (Xofigo® [59]). The targeted delivery of ^{223}Ra to various organs can be achieved by creating a stable conjugate with nanomaterials, which is then transported using the biological vector, to the desired organ. Thus, we recently demonstrated the possibility of sorption of ^{223}Ra on NDs with grafted derivatives of amino acids, but the maximum sorption under the studied conditions was only 10% [60].

Studies of Ra(II) sorption showed that all the CNMs samples studied did not sorb Ra(II) in 60 min in an aqueous solution with pH 6, with the exception of rGiO, on which sorption reached 60%. Upon contact of the sorbent with Ra(II), it was shown that in saline, PBS and PBS + BSA, desorption from 35 to 70% was observed within 30 min. It can be noted that sorption of alkaline earth metals Mg(II), Ca(II), Sr(II) and Ba(II) on rGiO was also observed [61], while it was shown that sorption increased with an increase in the ionic radius. This demonstrates the difficulties of the direct use of the $^{223}Ra(II)@rGiO$ conjugate as an RP, however, the lack of complete desorption indicates the prospects for studying rGiO as a carrier of ^{223}Ra.

4. Conclusion

In this work, the sorption behavior of ^{99m}Tc, ^{207}Bi, ^{90}Y, and ^{226}Ra on commercial and modified NDs, rGiO, and MWCNTs samples was studied. It was found that the CNMs investigated sorb up to 90% of Tc(VII), however, its quantitative desorption occurs in physiological saline. Tc(IV) is efficiently sorbed by the oxidized surface of CNMs at > 90%, while its desorption in PBS + BSA solution does not exceed 5%. This allows the use of the studied ND, rGiO and MWCNTs with oxygen-containing groups on their surface for targeted delivery of RP with Tc(IV). The sorption of Bi(III) on the CNMs studied ranged from 80 to 100%, while its desorption in BSA in PBS for ND, ND-COOH and rGiO did not exceed 10%, and for CNMs without oxygen-containing groups, up to 30%. It was shown that the kinetics of sorption of Y(III) is slower than for Bi(III) and depends on the morphology of CNMs. Desorption in PBS + BSA solution in 1 h raised to 35% from the surface of ND, and 15% from the surface of rGiO. The possibility of controlled release of Bi(III) and Y(III) isotopes from the CNMs surface has been established, and creates the prerequisites for their variable use in the RP composition. It was shown that rGiO is a promising carrier of Ra(II) for RP, however, additional studies are required to increase the strength of binding of the radionuclide to rGiO.

The results indicate that the use of CNMs for sorption of radionuclides in order to create RP with targeted delivery is quite promising. The possibility of selecting the sorbed radionuclide depending on the

Fig. 7. Desorption of Y(III) in PBS + BSA solution at 25 °C, 100 μg/mL CNM content.

type of material, functionalization of its surface, and controlled release in a biological medium has been revealed, which allows CNMs to be considered as multimodal carriers in RP. The patterns of sorption behavior of the studied isotopes shown on CNMs will contribute to the selection of optimal conditions for sorption of other nuclides used in nuclear medicine.

CRediT authorship contribution statement

Andrey G. Kazakov: Investigation, Writing - review & editing. **Bogdan L. Garashchenko:** Investigation, Writing - review & editing. **Ruslan Yu. Yakovlev:** Conceptualization, Investigation, Writing - review & editing. **Sergey E. Vinokurov:** Resources, Writing - review & editing. **Stepan N. Kalmykov:** Resources. **Boris F. Myasoedov:** Writing - review & editing, Supervision.

Acknowledgements

Appendix A. Supplementary data

Supplementary data to this article can be found online at https://doi.org/10.1016/j.diamond.2020.107752.

References

[1] B. Garg, C.-H. Sung, Y.-C. Ling, Graphene-based nanomaterials as molecular imaging agents, Wiley Interdiscip. Rev. Nanomedicine Nanobiotechnology. 7 (2015) 737–758, https://doi.org/10.1002/wnan.1342.

[2] J.A. Barreto, W. O'Malley, M. Kubeil, B. Graham, H. Stephan, L. Spiccia, Nanomaterials: applications in cancer imaging and therapy, Adv. Mater. 23 (2011), https://doi.org/10.1002/adma.201100140.

[3] D. Chen, C.A. Dougherty, K. Zhu, H. Hong, Theranostic applications of carbon nanomaterials in cancer: focus on imaging and cargo delivery, J. Control. Release 210 (2015) 230–245, https://doi.org/10.1016/j.jconrel.2015.04.021.

[4] T. Yamashita, K. Yamashita, H. Nabeshi, T. Yoshikawa, Y. Yoshioka, S. ichi Tsunoda, Y. Tsutsumi, Carbon nanomaterials: efficacy and safety for nanomedicine, Materials (Basel) 5 (2012) 350–363, https://doi.org/10.3390/ma5020350.

[5] G. Hong, J.Z. Wu, J.T. Robinson, H. Wang, B. Zhang, H. Dai, Three-dimensional imaging of single nanotube molecule endocytosis on plasmonic substrates, Nat. Commun. 3 (2012) 700–709, https://doi.org/10.1038/ncomms1698.

[6] R.G. Mendes, A. Bachmatiuk, B. Büchner, G. Cuniberti, M.H. Rümmeli, Carbon nanostructures as multi-functional drug delivery platforms, J. Mater. Chem. B 1 (2013) 401–428, https://doi.org/10.1039/c2tb00085g.

[7] D. Peer, J.M. Karp, S. Hong, O.C. Farokhzad, R. Margalit, R. Langer, Nanocarriers as an emerging platform for cancer therapy, Nat. Nanotechnol. 2 (2007) 751–760, https://doi.org/10.1038/nnano.2007.387.

[8] E.K. Chow, X.Q. Zhang, M. Chen, R. Lam, E. Robinson, H. Huang, D. Schaffer, E. Osawa, A. Goga, D. Ho, Nanodiamond therapeutic delivery agents mediate enhanced chemoresistant tumor treatment, Sci. Transl. Med. 3 (2011), https://doi.org/10.1126/scitranslmed.3001713.

[9] S. Ozdemir, E. Kilinc, K.S. Celik, V. Okumus, M. Soylak, Simultaneous preconcentrations of Co^{2+}, Cr^{6+}, Hg^{2+} and Pb^{2+} ions by Bacillus altitudinis immobilized nanodiamond prior to their determinations in food samples by ICP-OES, Food Chem. 215 (2017) 447–453, https://doi.org/10.1016/j.foodchem.2016.07.055.

[10] W.A.W. Ibrahim, H.R. Nodeh, M.M. Sanagi, Graphene-based materials as solid phase extraction sorbent for trace metal ions, organic compounds, and biological sample preparation, Crit. Rev. Anal. Chem. 46 (2016) 267–283, https://doi.org/10.1080/10408347.2015.1034354.

[11] A.A. Gouda, S.M. Al Ghannam, Impregnated multiwalled carbon nanotubes as efficient sorbent for the solid phase extraction of trace amounts of heavy metal ions in food and water samples, Food Chem. 202 (2016) 409–416, https://doi.org/10.1016/j.foodchem.2016.02.006.

[12] K. Yang, L. Zhu, B. Xing, Adsorption of polycyclic aromatic hydrocarbons by carbon nanomaterials, Environ. Sci. Technol. 40 (2006) 1855–1861, https://doi.org/10.1021/es052208w.

[13] B. Pan, B. Xing, Adsorption mechanisms of organic chemicals on carbon nanotubes, Environ. Sci. Technol. 42 (2008) 9005–9013, https://doi.org/10.1021/es801777n.

[14] J. Jeon, Review of therapeutic applications of radiolabeled functional nanomaterials, Int. J. Mol. Sci. 20 (2019), https://doi.org/10.3390/ijms20092323.

[15] A. Kamkaew, E.B. Ehlerding, W. Cai, Radiopharmaceutical chemistry, Radiopharm. Chem. (2019), https://doi.org/10.1007/978-3-319-98947-1.

[16] S.Y. Hong, G. Tobias, K.T. Al-Jamal, B. Ballesteros, H. Ali-Boucetta, S. Lozano-Perez,

[17] P.D. Nellist, R.B. Sim, C. Finucane, S.J. Mather, M.L.H. Green, K. Kostarelos, B.G. Davis, Filled and glycosylated carbon nanotubes for in vivo radioemitter localization and imaging, Nat. Mater. 9 (2010) 485–490, https://doi.org/10.1038/nmat2766.

[17] W. Qi, Z. Li, J. Bi, J. Wang, J. Wang, T. Sun, Y. Guo, W. Wu, Biodistribution of co-exposure to multi-walled carbon nanotubes and nanodiamonds in mice, Nanoscale Res. Lett. 7 (2012) 1–9, https://doi.org/10.1186/1556-276X-7-473.

[18] O.O. Peltek, A.R. Muslimov, M.V. Zyuzin, A.S. Timin, Current outlook on radionuclide delivery systems: from design consideration to translation into clinics, J. Nanobiotechnology. 17 (2019) 1–34, https://doi.org/10.1186/s12951-019-0524-9.

[19] S. Rojas, J.D. Gispert, R. Martín, S. Abad, C. Menchón, D. Pareto, V.M. Víctor, M. Álvaro, H. García, J.R. Herance, Biodistribution of amino-functionalized diamond nanoparticles. In vivo studies based on ^{18}F radionuclide emission, ACS Nano 5 (2011) 5552–5559, https://doi.org/10.1021/nn200986z.

[20] L. Chen, X. Zhong, X. Yi, M. Huang, P. Ning, T. Liu, C. Ge, Z. Chai, Z. Liu, K. Yang, Radionuclide ^{131}I labeled reduced graphene oxide for nuclear imaging guided combined radio- and photothermal therapy of cancer, Biomaterials 66 (2015) 21–28, https://doi.org/10.1016/j.biomaterials.2015.06.043.

[21] S. Zhang, K. Yang, L. Feng, Z. Liu, In vitro and in vivo behaviors of dextran functionalized graphene, Carbon N. Y. 49 (2011) 4040–4049, https://doi.org/10.1016/j.carbon.2011.05.056.

[22] D.W. Jiang, C. Peng, Y.H. Sun, L.N. Jia, J.B. Li, L. Zhang, Study on technetium-99m labeling of graphene oxide nanosheets through click chemistry-^{99m}Tc labeling of graphene oxide nanosheets, Nucl. Sci. Tech. 26 (2015) 1–5, https://doi.org/10.13538/j.1001-8042/nst.26.040301.

[23] S. Vardharajula, S.Z. Ali, P.M. Tiwari, E. Eroğlu, K. Vig, V.A. Dennis, S.R. Singh, Functionalized carbon nanotubes: biomedical applications, Int. J. Nanomedicine 7 (2012) 5361–5374, https://doi.org/10.2147/IJN.S35832.

[24] K.B. Hartman, D.K. Hamlin, D.S. Wilbur, L.J. Wilson, $^{211}AtCl@US$-tube nanocapsules: a new concept in radiotherapeutic-agent design, Small 3 (2007) 1496–1499, https://doi.org/10.1002/smll.200700153.

[25] A. Ruggiero, C.H. Villa, J.P. Holland, S.R. Sprinkle, C. May, J.S. Lewis, D.A. Scheinberg, M.R. McDevitt, Imaging and treating tumor vasculature with targeted radiolabeled carbon nanotubes, Int. J. Nanomedicine 5 (2010) 783–802, https://doi.org/10.2147/IJN.S13300.

[26] X. Lv, J. Xu, G. Jiang, X. Xu, Removal of chromium(VI) from wastewater by nanoscale zero-valent iron particles supported on multiwalled carbon nanotubes, Chemosphere 85 (2011) 1204–1209, https://doi.org/10.1016/j.chemosphere.2011.09.005.

[27] J. Xu, Z. Cao, Y. Zhang, Z. Yuan, Z. Lou, X. Xu, X. Wang, A review of functionalized carbon nanotubes and graphene for heavy metal adsorption from water: preparation, application, and mechanism, Chemosphere 195 (2018) 351–364, https://doi.org/10.1016/j.chemosphere.2017.12.061.

[28] R.Y. Yakovlev, N.N. Dogadkin, I.I. Kulakova, G.V. Lisichkin, N.B. Leonidov, V.P. Kolotov, Determination of impurities in detonation nanodiamonds by gamma activation analysis method, Diam. Relat. Mater. 55 (2015) 77–86, https://doi.org/10.1016/j.diamond.2015.03.010.

[29] G.V. Lisichkin, I.I. Kulakova, Y.A. Gerasimov, A.V. Karpukhin, R.Y. Yakovlev, Halogenation of detonation-synthesised nanodiamond surfaces, Mendeleev Commun 19 (2009) 309–310, https://doi.org/10.1016/j.mencom.2009.11.004.

[30] A.S. Solomatin, R.Y. Yakovlev, V.V. Teplova, N.I. Fedotcheva, M.N. Kondrachova, I.I. Kulakova, N.B. Leonidov, Effect of detonation nanodiamond surface composition on physiological indicators of mitochondrial functions, J. Nanopart. Res. 20 (2018), https://doi.org/10.1007/s11051-018-4297-0.

[31] P. Pichestapong, W. Sriwiang, U. Injarean, Separation of Yttrium-90 from Strontium-90 by extraction chromatography using combined Sr resin and RE resin, Energy Procedia 89 (2016) 366–372, https://doi.org/10.1016/j.egypro.2016.05.048.

[32] M.A. Motaleb, Preparation and biodistribution of ^{99m}Tc-lomefloxacin and ^{99m}Tc-ofloxacin complexes, J. Radioanal. Nucl. Chem. 272 (2007) 95–99, https://doi.org/10.1007/s10967-006-6786-3.

[33] M.G.L. Olthof, M.A. Tryfonidou, M. Dadsetan, W.J.A. Dhert, M.J. Yaszemski, D.H.R. Kempen, L. Lu, *In vitro* and *in vivo* correlation of bone morphogenetic protein-2 release profiles from complex delivery vehicles, Tissue Eng. - Part C Methods. 24 (2018) 379–390, https://doi.org/10.1089/ten.tec.2018.0024.

[34] H. Shibata, Fabrication and functionalization of inorganic materials using amphiphilic molecules, J. Oleo Sci. 66 (2017) 103–111, https://doi.org/10.5650/jos.ess16194.

[35] W.G. Jin, W. Chen, P.H. Xu, X.W. Lin, X.C. Huang, G.H. Chen, F. Lu, X.M. Chen, An exceptionally water stable metal–organic framework with amide-functionalized cages: selective CO_2/CH_4 uptake and removal of antibiotics and dyes from water, Chem. - A Eur. J. 23 (2017) 13058–13066, https://doi.org/10.1002/chem.201701884.

[36] V.Y. Dolmatov, Detonation-synthesis nanodiamonds: synthesis, structure, properties and applications, Russ. Chem. Rev. 76 (2007) 339–360, https://doi.org/10.1070/rc2007v076n04abeh003643.

[37] C. Xie, N. Tsakok, N. Taylor, K. Partington, Imaging of brown tumours: a pictorial review, Insights Imaging 10 (2019), https://doi.org/10.1186/s13244-019-0757-z.

[38] P.J. Blower, A nuclear chocolate box: the periodic table of nuclear medicine, Dalt. Trans. 44 (2015) 4819–4844, https://doi.org/10.1039/c4dt02846e.

[39] P. Rajec, M. Galamboš, M. Daňo, O. Rosskopfová, M. Čaplovičová, P. Hudec, M. Horňáček, I. Novák, D. Berek, Čaplovič, Preparation and characterization of adsorbent based on carbon for pertechnetate adsorption, J. Radioanal. Nucl. Chem. 303 (2015) 277–286, https://doi.org/10.1007/s10967-014-3303-y.

[40] M. Daňo, E. Viglašová, M. Galamboš, P. Rajec, I. Novák, Sorption behaviour of pertechnetate on oxidized and reduced surface of activated carbon, J. Radioanal.

Nucl. Chem. 314 (2017) 2219–2227, https://doi.org/10.1007/s10967-017-5532-3.

[41] Petrović, A. Đukić, K. Kumrić, B. Babić, M. Momčilović, N. Ivanović, L. Matović, Mechanism of sorption of pertechnetate onto ordered mesoporous carbon, J. Radioanal. Nucl. Chem. 302 (2014) 217–224, https://doi.org/10.1007/s10967-014-3249-0.

[42] S. El-Wear, K.E. German, V.F. Peretrukhin, Sorption of technetium on inorganic sorbents and natural minerals, J. Radioanal. Nucl. Chem. Artic. 157 (1992) 3–14, https://doi.org/10.1007/BF02039772.

[43] R.V. Hercigonja, D.D. Maksin, A.B. Nastasović, S.S. Trifunović, P.B. Glodić, A.E. Onjia, Adsorptive removal of technetium-99 using macroporous poly(GMA-co-EGDMA) modified with diethylene triamine, J. Appl. Polym. Sci. 123 (2012) 1273–1282, https://doi.org/10.1002/app.34693.

[44] N. Petrova, A. Zhukov, F. Gareeva, A. Koscheev, I. Petrov, O. Shenderova, Interpretation of electrokinetic measurements of nanodiamond particles, Diam. Relat. Mater. 30 (2012) 62–69, https://doi.org/10.1016/j.diamond.2012.10.004.

[45] K. Schwochau, Technetium: Chemistry and Radiopharmaceutical Applications, Wiley, 2000.

[46] F.L. Thorp-Greenwood, M.P. Coogan, Multimodal radio- (PET/SPECT) and fluorescence imaging agents based on metallo-radioisotopes: current applications and prospects for development of new agents, J. Chem. Soc. Dalt. Trans. 40 (2011) 6129–6143, https://doi.org/10.1039/c0dt01398f.

[47] Y.S. Kim, M.W. Brechbiel, An overview of targeted alpha therapy, Tumor Biol. 33 (2012) 573–590, https://doi.org/10.1007/s13277-011-0286-y.

[48] K.E. Baidoo, D.E. Milenic, M.W. Brechbiel, Methodology for labeling proteins and peptides with lead-212 (^{212}Pb), Nucl. Med. Biol. 40 (2013) 592–599, https://doi.org/10.1016/j.nucmedbio.2013.01.010.

[49] T.L. Rosenblat, M.R. McDevitt, D.A. Mulford, N. Pandit-Taskar, C.R. Divgi, K.S. Panageas, M.L. Heaney, S. Chanel, A. Morgenstern, G. Sgouros, S.M. Larson, D.A. Scheinberg, J.G. Jurcic, Sequential cytarabine and α-particle immunotherapy with bismuth-213-lintuzumab (HuM195) for acute myeloid leukemia, Clin. Cancer Res. 16 (2010) 5303–5311, https://doi.org/10.1158/1078-0432.CCR-10-0382.

[50] B.L. Garashchenko, V.A. Korsakova, R.Y. Yakovlev, Radiopharmaceuticals based on alpha emitters: preparation, properties, and application, Phys. At. Nucl. 81 (2018) 1515–1525, https://doi.org/10.1134/S1063778818100071.

[51] A. Romer, D. Seiler, N. Marincek, P. Brunner, M.T. Koller, Q.K.T. Ng, H.R. Maecke, J. Müller-Brand, C. Rochlitz, M. Briel, C. Schindler, M.A. Walter, Somatostatin-based radiopeptide therapy with [^{177}Lu-DOTA]-TOC versus [^{90}Y-DOTA]-TOC in neuroendocrine tumours, Eur. J. Nucl. Med. Mol. Imaging 41 (2014) 214–222,

[52] S. Walrand, F. Jamar, I. Mathieu, J. Camps, M. Lonneux, M. Sibomana, D. Labar, C. Michel, S. Pauwels, Quantitation in PET using isotopes emitting prompt single gammas: application to yttrium-86, Eur. J. Nucl. Med. Mol. Imaging 30 (2003) 354–361, https://doi.org/10.1007/s00259-002-1068-y.

https://doi.org/10.1007/s00259-013-2559-8.

[53] I. Fenoglio, G. Greco, M. Tomatis, J. Muller, E. Raymundo-Piñero, F. Béguin, A. Fonseca, J.B. Nagy, D. Lison, B. Fubini, Structural defects play a major role in the acute lung toxicity of multiwall carbon nanotubes: physicochemical aspects, Chem. Res. Toxicol. 21 (2008) 1690–1697, https://doi.org/10.1021/tx800100s.

[54] X.L. Tan, D. Xu, C.L. Chen, X.K. Wang, W.P. Hu, Adsorption and kinetic desorption study of $^{152+154}$Eu(III) on multiwall carbon nanotubes from aqueous solution by using chelating resin and XPS methods, Radiochim. Acta 96 (2008) 23–29, https://doi.org/10.1524/ract.2008.1457.

[55] R. Singh, D. Pantarotto, L. Lacerda, G. Pastorin, C. Klumpp, M. Prato, A. Bianco, K. Kostarelos, Tissue biodistribution and blood clearance rates of intravenously administered carbon nanotube radiotracers, Proc. Natl. Acad. Sci. U. S. A. 103 (2006) 3357–3362, https://doi.org/10.1073/pnas.0509009103.

[56] J.-H. Liu, S.-T. Yang, H. Wang, Y. Chang, A. Cao, Y. Liu, Effect of size and dose on the biodistribution of graphene oxide in mice, Nanomedicine 7 (2012) 1801–1812, https://doi.org/10.2217/nnm.12.60.

[57] R.Y. Yakovlev, A.S. Solomatin, N.B. Leonidov, I.I. Kulakova, G.V. Lisichkin, Detonation diamond—a perspective carrier for drug delivery systems, Russ. J. Gen. Chem. 84 (2014) 379–390, https://doi.org/10.1134/S1070363214020406.

[58] G.M. Bhalerao, A.K. Sinha, V. Sathe, Defect-dependent annealing behavior of multi-walled carbon nanotubes, Physica E: Low-dimensional Systems and Nanostructures 41 (2008) 54–59, https://doi.org/10.1016/j.physe.2008.06.006.

[59] R. Gallicchio, P.A. Mastrangelo, A. Nardelli, P.P. Mainenti, A.P. Colasurdo, M. Landriscina, G. Guglielmi, G. Storto, Radium-223 for the treatment of bone metastases in castration-resistant prostate cancer: when and why, Tumori J 105 (2019) 367–377, https://doi.org/10.1177/0300891619851376.

[60] B.L. Garashchenko, N.N. Dogadkin, N.E. Borisova, R.Y. Yakovlev, Sorption of ^{223}Ra and ^{211}Pb on modified nanodiamonds for potential application in radiotherapy, J. Radioanal. Nucl. Chem. 318 (2018) 2415–2423, https://doi.org/10.1007/s10967-018-6330-2.

[61] Z. Sofer, L. Wang, K. Klímová, M. Pumera, Highly selective uptake of Ba^{2+} and Sr^{2+} ions by graphene oxide from mixtures of IIA elements, RSC Adv. 4 (2014) 26673–26676, https://doi.org/10.1039/C4RA02640C.